Songklanakarin J. Sci. Technol.
35 (2), 203-212, Mar. - Apr. 2013

SJST SONGKLANAKARIN JOURNAL OF SCIENCE AND TECHNOLOGY
http://www.sjst.psu.ac.th

Original Article

Influence of nozzle arrangement on flow and heat transfer characteristics of arrays of circular impinging jets

Makatar Wae-hayee, Perapong Tekasakul, and Chayut Nuntadusit*

Energy Technology Research Center and Department of Mechanical Engineering, Faculty of Engineering, Prince of Songkla University, Hat Yai, Songkhla, 90112 Thailand.

Received 31 January 2012; Accepted 1 February 2013

Abstract

The effect of jet arrangements on flow and heat transfer characteristics was experimentally and numerically investigated for arrays of impinging jets. The air jets discharge from round orifices and perpendicularly impinge on a surface within a rectangular duct. Both the in-line and staggered arrangements, which have an array of 6×4 nozzles, were examined. A jet-to-plate distance (H) and jet-to-jet distance (S) were fixed at H=2D and S=3D, respectively (where D is the round orifice diameter). The experiments were carried out at jet Reynolds number Re=5,000, 7,500 and 13,400. Temperature distributions on the impingement surface were measured using a Thermochromic Liquid Crystal sheet, and Nusselt number distributions were evaluated using an image processing method. The flow characteristics on the impingement surface were visualized using the oil film technique. The numerical simulation employed to gain insight into the fluid flow of jets between the orifice plate and the impingement wall was via computational fluid dynamics. The results reveal that the effect of crossflow on the impinging jets for the staggered arrangement is stronger than that in the case of in-line arrangement. In the latter case of in-line arrangement, the crossflow could pass throughout the passage between the rows of jets, whereas in the former case the crossflow was hampered by the downstream jets. The average Nusselt number of the in-line arrangement is higher than that of the staggered arrangement by approx. 13-20% in this study.

Keywords: array of impinging jets, in-line and staggered arrangement, crossflow, thermochromic liquid crystal sheet (TLCs), oil film technique, CFD

1. Introduction

Jet impingement is a high-performance technique for heat transfer enhancement in thermal equipment. It has also been used in industrial processes for heating, cooling and drying. Since the heat transfer rate is very high at the area where the jet directly impinges on, it provides rapid cooling or heating on the local heat transfer area (Ashforth-Frost and Jambunathan, 1996; Colucci and Viskanta, 1996). However, many thermal industrial applications have large surface area of heat transfer such as combustor chamber wall and gas turbine blade cooling, steel and glass quenching, and textile and paper drying. When high and uniform heat transfer rate is required over the entire surfaces, multiple impinging jets or array of impinging jets are applied.

An important factor affecting flow and heat transfer characteristics of multiple impinging jets in a confined space is the crossflow. Crossflow is defined as fluid flow in the perpendicular direction to the jet impingement flow. It can be formed by either external flow or accumulating spent jet flow. In the case of multiple impinging jets in a confined space, the spent jet is accumulated from upstream to the downstream end of the channel. The flow rate, or velocity of the crossflow, is thus increased from upstream to the downstream of the channel. Consequently, the flow and heat transfer of the impinging jets located at downstream of the channel is signi-

* Corresponding author.
Email address: chayut@me.psu.ac.th

ficantly influenced by the crossflow (Viskanta, 1993).

Various previous studies have shown the effects of crossflow on the flow and heat transfer characteristics of multiple impinging jets. Florschuetz *et al*. (1981) investigated the Nusselt number correlation for both the in-line and staggered arrangements in case of jet-to-jet distance of $S>4D$ (where D is the nozzle diameter). Brizzi *et al*. (2000) illustrated flow and temperature patterns on the impingement surface of an array of jets with in-line arrangement and confirmed that flow patterns correspond to the temperature distributions. Katti and Prabhu (2008) studied heat transfer on an impingement surface under an array of jets, also in an in-line arrangement. Results shown by their study are that the heat transfer rate under jet-to-jet distance in spanwise direction for $S=4D$ is higher than for either $S=2D$ or $S=6D$. However, the optimal jet-to-jet distance in streamwise direction has not been reported.

Not many works have been conducted on the flow characteristics of multiple impinging jets with the effect of crossflow (Carcasci, 1999; Brizzi *et al*., 2000). It is difficult to identify the interaction between the crossflow and the jet in the case of multiple impingement flows. To illustrate the ratio of jet velocity to the crossflow velocity influencing the flow and heat transfer of impinging jet, a single impinging jet with simulated crossflow was experimentally investigated (Bouchez and Goldstein, 1975; Goldstein and Behbahani, 1982; Nakabe *et al*., 1998; Barata and Durao, 2004). Recently, a numerical simulation has also been used for a flow field study of a single impinging jet with simulated crossflow (Shi *et al*., 2003; Yang and Wang, 2005). In order to illustrate the interaction between the jet and the crossflow in case of multiple impingement flows in the present study, numerical simulation has been adopted.

In more recent works is was shown that in order to enhance the heat transfer rate under an array of impinging jets with in-line arrangement, an impingement surface with mounted ribs was applied (Rallabandi *et al.* 2010; Xing *et al.,* 2011; Caliskan and Baskaya, 2012). However, there had been no investigations on staggered arrangement in their works. Hoberg *et al.* (2010) investigated experimentally the impinging jet array together with the use of effusion holes in an effort to enhance the heat transfer rate reduced in the crossflow by a staggered arrangement. Nevertheless, this investigation was observed solely for an average heat transfer without details on its flow characteristics and local heat transfer. A more vigorous study in the work on the flow characteristics and heat transfer to identify and illustrate the effects of crossflow on jet impingement arrays with comparison of in-line and staggered arrangement is thus needed.

The aim of the present study is to investigate the effect of nozzle arrangement for array of impinging jets in case of low jet-to-plate distances. The in-line and staggered arrangement were experimentally and numerically conducted. The temperature distribution on the impingement surface was investigated using a Thermochromic Liquid Crystal sheet (TLCs), and the Nusselt number distribution was evaluated using an image processing method. The characteristic of the flow on the impingement surface was visualized employing the oil film technique. The numerical simulation employed to gain insight into the fluid flow of multiple impinging jets under crossflow was via a commercial ANSYS ver. 12.0, Fluent software.

2. Experimental Setup and Method

2.1 Experimental model and parameters

An experimental model displaying jets discharging from round orifice and impinging normal to the opposite surface in a confined rectangular duct is shown in Figure 1. Crossflow is generated by accumulation of spent jet (jet after impinging) at the upstream terminal that flows out to the exit at the other end of the duct. A Cartesian coordinate system with its origin allocated at the impingement surface is as shown in Figure 1 and 2. The Y-axis is normal to the target

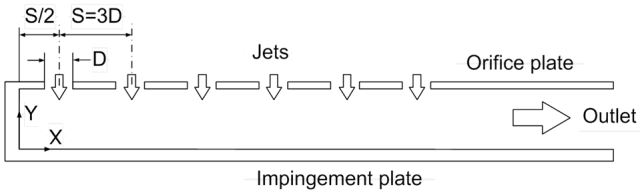

Figure 1. Experimental model of array of impinging jets.

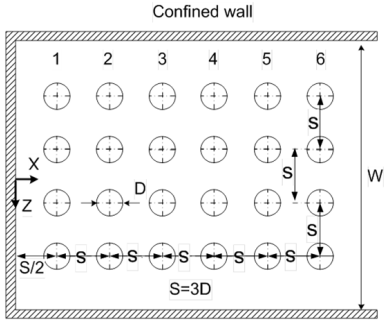

(a)

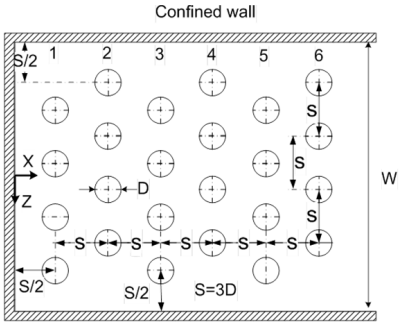

(b)

Figure 2. Experimental model of jet arrangement (D=13.2 mm, W=180 mm): (a) In-line arrangement and (b) staggered arrangement.

surface, while the X- and the Z-axes are along the streamwise and the spanwise directions of the crossflow, respectively.

The arrays of jet arrangements are as shown in Figure 2 which depict the in-line configuration in (a) and the staggered arrangement in (b). The diameter D of each round orifice, having a smooth square-edge nozzle through a plate of 2 mm thickness, is 13.2 mm. Both jet arrangements have the same array of 6×4 jet holes; 6 on the streamwise and 4 on the spanwise direction. Both arrangements have constant jet-to-jet distance S=3D and jet-to-plate distance H=2D. In the case of staggered arrangement, as shown in Figure 2(b), a jet-to-sidewall distance of S/2 (=1.5D) is assigned to the nearest nozzles to the wall. Dimensions of the duct for the staggered arrangement, both height and width, are thus fixed by these requirements. The same sidewall distance is assigned to the in-line arrangement, and hence the same duct dimension is applicable for both configurations. The experiments were carried out at jet Reynolds number of Re=5,000, 7,500 and 13,400 that calculate jet velocity at center of nozzle outlet.

2.2 Experimental setup

The schematic diagram and photographs of the experimental apparatus are shown in Figure 3. A 3-HP blower (Artith Machinery, Av-D1216, Thailand) accelerates the air which flows through a temperature controlled chamber equipped with a 2-kW heater (Sangi Electric, FU-4010, Thailand). The heated air is then forced through a calibrated orifice flow meter and into a jet chamber having a cross-section of 360 mm × 360 mm and a height of 850 mm. The jet chamber is equipped with two layers of perforated plates and two layers of mesh plates to ensure a uniform flow field when the air approaches the orifice plate. Finally, the compressed air in the chamber forces through the jet orifice and enters the test section.

The test section is directly mounted on top of the jet chamber, as shown in Figure 3. Under all experimental conditions, the jet temperature was controlled at 27°C by a temperature controller (Shinko, JCS-33A, Japan) and a power controller (Sangi Electric, SCR-1A030, Thailand). In these experiments, temperature variations of the jet can be controlled within 0.2°C.

2.3 Heat transfer measurement

Figure 3 also outlines details of the test section for heat transfer measurement. Air with constant temperature is discharged through the orifice plate and impinges upon the heat transfer surface. The heat transfer surface, made of stainless steel foil (30 μm thick), is attached with the TLCs (Omega, LCS-95, U.S.A.) on the rear side of the impingement surface. The stainless steel foil is stretched between a couple of copper bus bars. The heat transfer surface is heated by a DC power supply (Silicon, WYK-15V50A-H, Thailand) that can supply a current up to 50 A through the copper bus bars. Electrical energy dissipated in the stainless steel foil can be calculated from:

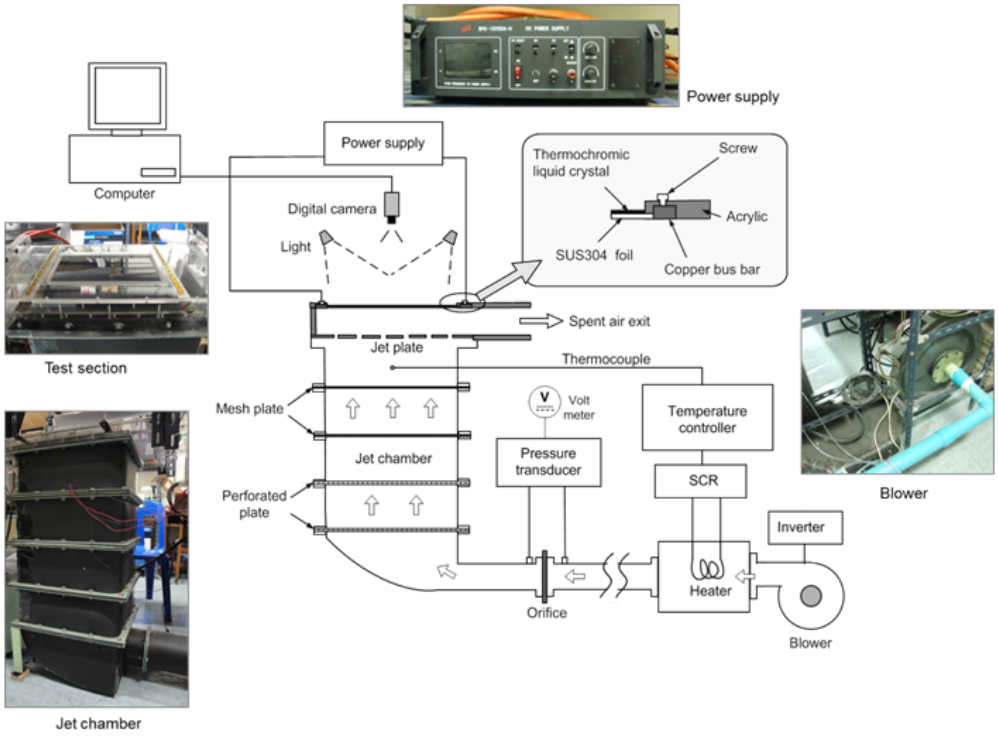

Figure 3. Schematic and photographs of the experimental apparatus.

$$\dot{Q}_{input} = I^2 \cdot R \quad (1)$$

where I is the electrical current, and R is the thermal eletrical resistance of the stainless steel foil.

The local heat transfer coefficient by forced convection of the jet, h, can be evaluated from:

$$h = \frac{\dot{Q}_{input} - \dot{Q}_{losses}}{A(T_w - T_j)} = \frac{\dot{q}_{input} - \dot{q}_r - \dot{q}_c}{T_w - T_j} \quad (2)$$

where A is area of stainless steel foil, $\dot{q}_r = \sigma\varepsilon_{TLC}(T_w - T_s)$ and $\dot{q}_c = h_c(T_w - T_s)$ are the heat losses to the environment by radiation and convection, respectively, T_w and T_j are the wall and jet temperatures, σ is the Stefan-Boltzman constant, ε_{TLC} is the emissive coefficient of the TLC sheet (Geers *et al*., 2008), T_s is the surrounding temperature, and h_c is the natural heat transfer coefficient calculated from natural convective heat transfer from the heat transfer surface to the surrounding.

The wall temperature (T_w) on the impingement surface was measured using the TLCs attached at the rear side of the jet impingement surface. A digital camera (Creative, Live Pro, 1,280×960 pixels, China) was used to capture color on the TLCs under manual brightness mode. Images of color pattern on the TLCs were converted from RGB (Red, Green and Blue) system to HSI (Hue, Saturation, and Intensity) system. The Hue (H) value provides a convenient way to correlate color of the TLCs to the temperature. The TLCs was calibrated under the same conditions of the experimental runs.

The local Nusselt number can be calculated from:

$$Nu = \frac{hD}{k} \quad (3)$$

where D is the round orifice diameter, and k is the jet thermal conductivity.

The average Nusselt number can be calculated from:

$$\overline{Nu} = \frac{\bar{h}D}{k} \quad (4)$$

where $\bar{h}$ is the average heat transfer coefficient, calculated from Equation 2 by replacing T_w with the average temperature on the impingement surface, $\overline{T_w}$. Details of the heat transfer measurement adopted here have been described in two recent studies, Nuntadusit *et al*. (2012a and b).

2.4 TLCs temperature calibration

Temperature calibration of the TLCs was carried out under similar experimental conditions as that applied to the test section, with same viewing angle and lighting in an effort to keep external factors constant. The calibration rig composes of layers of materials and equipment, respectively, a 75×105 mm acrylic back-plate (10 mm thick, acting as thermal insulator), a thin coil heater (Kyohritsu, 80 Ω, 12 VDC, Japan), an aluminum plate (3 mm thick), four thermocouples, and the TLC sheet to be calibrated, as schematically shown in Figure 4, left view. A DC current was constantly applied to the thin coil heater by a DC power supply (KBM Engineering, PS-3002, Thailand). The maximum average temperature of close to 40°C is measured via four wires of the thermocouples

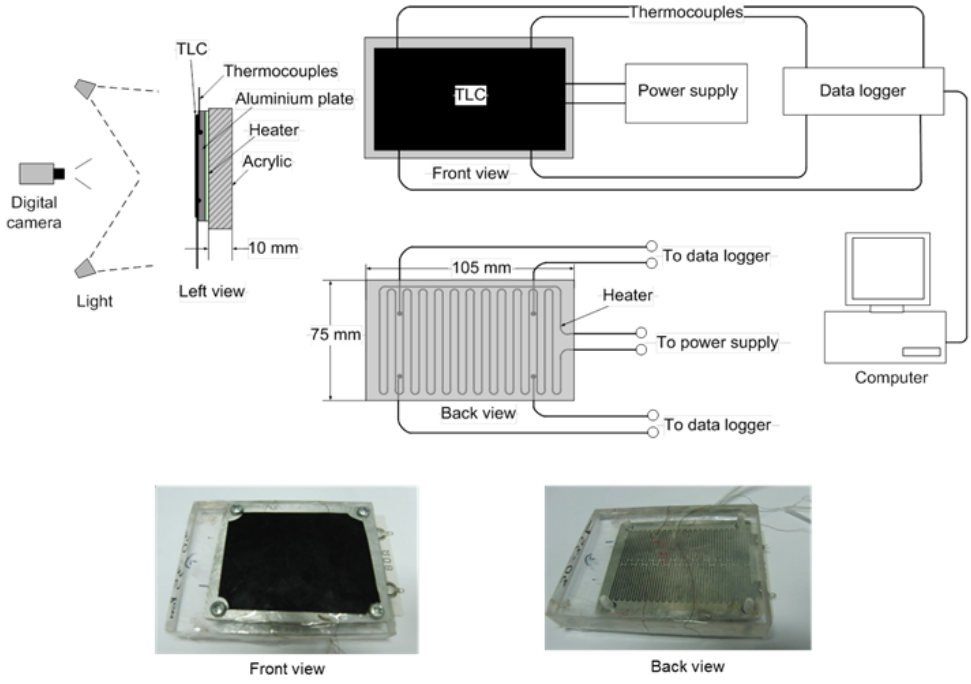

Figure 4. Schematic and photographs of the calibration rig.

mounted at assigned locations on the aluminum plate. Colors on the TLCs and temperatures were simultaneously recorded when an average temperature becomes steady. The electrical current thereafter was gradually decreased to yield lower temperatures. Calibration data were recorded in 0.2°C decremented steps as average temperature until it approached 27°C. Calibration was carried out on five different locations on the calibration rig positioned on the impingement surface. Relationship of the recorded temperature versus the normalized hue value from the color change observations is plotted in Figure 5 for all calibration positions.

2.5 Flow visualization on the impinged surface

Flow visualization on the impingement surface was carried out using the oil film technique. The oil mixture was prepared by mixing 20 g of liquid paraffin with 8.5 g of titanium dioxide and 3.5 g of oleic acid. A transparent plastic plate was used as the jet impingement wall and was uniformly painted coated by the oil. The same camera that has been employed throughout was used to record oil film patterns on the impingement surface at a 30-second time interval. The oil film image was captured in RGB system, as that employed in capturing the TLCs image.

2.6 Numerical simulation

Flow characteristics of the impinging jet in the confined channel were numerically simulated using the computational fluid dynamics (CFD) technique. Commercial package ANSYS (ver. 12.0) was used in this present study. The numerical model was identical to the experimental model schematically shown in Figure 6. Computations were conducted by solving continuity and Navier-stokes equations under existing boundary conditions. This k-ε turbulence model with general wall-function mode has been used in solving many numerical simulation problems (Shi *et al*., 2003;

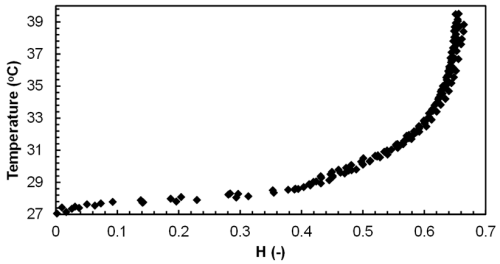

Figure 5. Temperature versus normalized hue value of TLCs calibration.

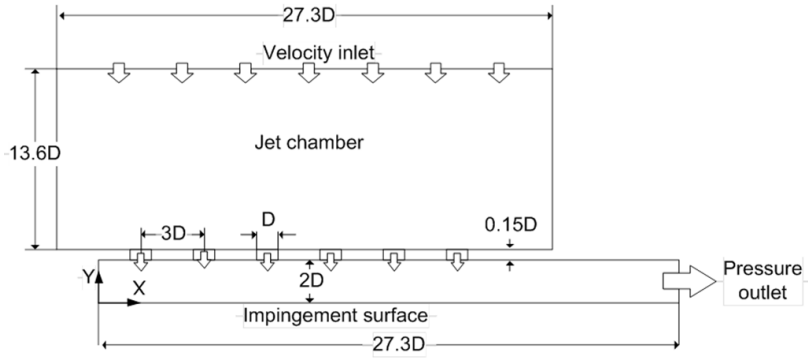

(a)

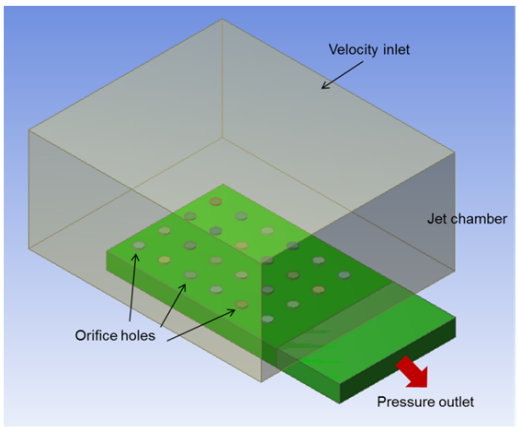

(b)

Figure 6. Domain of numerical simulation: (a) Schematic of domain and (b) 3-D numerical domain.

Yang and Wang, 2005).

Figure 7 details the internal grid used in this computation domain. The non-uniform grid system was finely generated for regions near the orifice holes and the impingement surface. A wall inflation function was used to concentrate the elements near the impingement surface. The impact of grid size on the static pressure on the impingement surface is shown in Figure 8. It can be noticed that the trend of static pressure having 1,603,186 and 1,934,306 cells exhibits less discrepancy than most others. The node with 1,603,186 cells was chosen for further simulations to minimize computation costs.

All boundary conditions applied were identical to those specified in experimental conditions. The inlet was regulated to give a constant inlet velocity of 0.36 m/s to maintain an average Reynolds number of the jets at *Re*= 13,400. The outlet pressure was kept constant at 1 atm. The solution method was based on SIMPLE algorithm with second order upwind for all spatial discretizations (Versteeg and Malalasekera, 1995). Solutions were considered converged when the normalized residual of all algebraic equations is less than the prescribed value of $1x10^{-4}$.

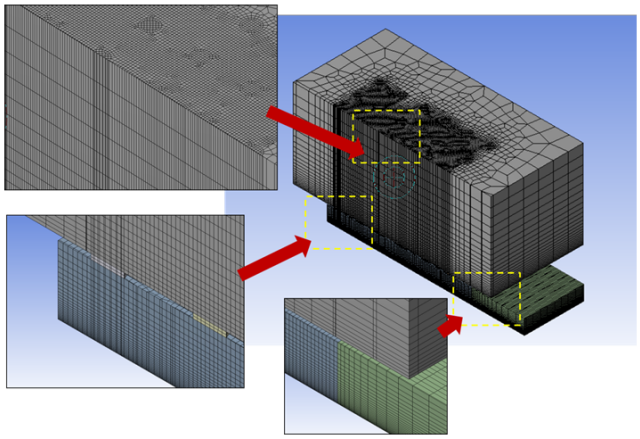

Figure 7. Internal grid system of in-line arrangement.

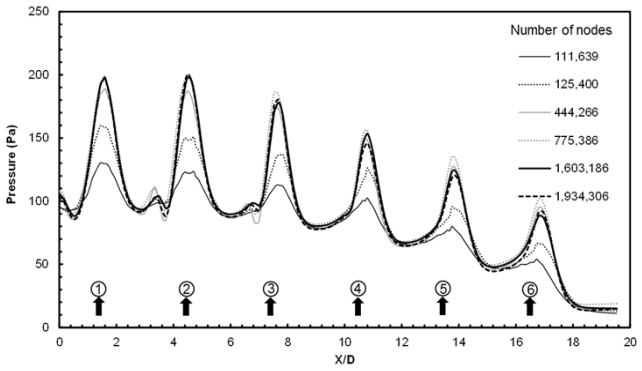

Figure 8. Effect of grid dependence on static pressure on the impingement surface for in-line arrangement (vertical arrows indicate the locations of column jets).

3. Results and Discussions

3.1 Flow characteristics

Flow characteristics derived from an array of impinging jets calculated using the CFD technique at *Re*=13,400 for the in-line and the staggered arrangements are shown in Figure 9 and 10, respectively. Velocity vectors and velocity contours of the flow field in the X-Y plane and the Y-Z plane are shown at major cross sections in the flow channel. In the case of in-line arrangement, the crossflow accumulated from the surface jets meanders between the rows of the jets to the

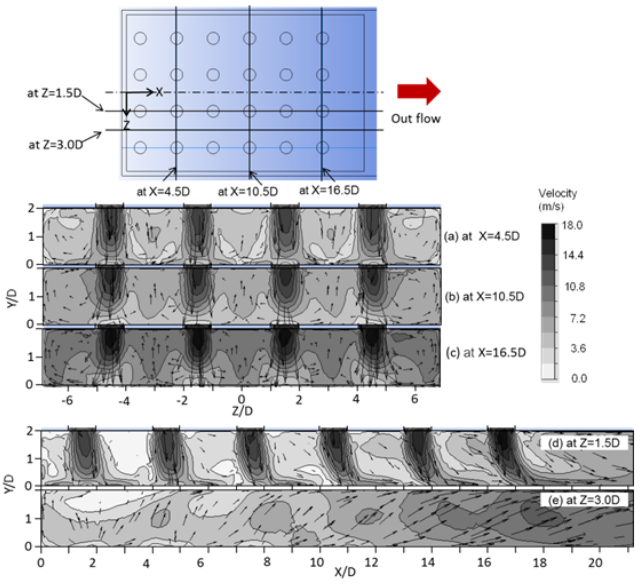

Figure 9. Flow characteristics in the case of in-line arrangement at Re=13,400.

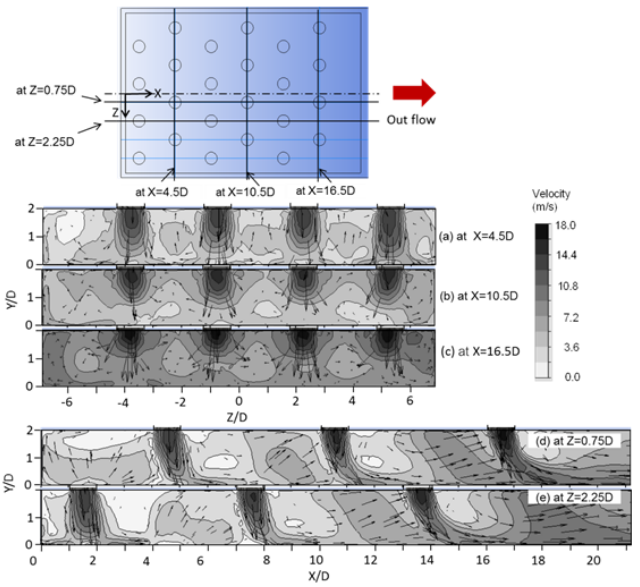

Figure 10. Flow characteristics in the case of staggered arrangement at Re=13,400.

channel exit. The crossflow velocity increases along the downstream direction to the channel exit, as notably shown in Figure 9(e). In Figure 9(d), due to the higher crossflow velocity further down the downstream region, deflection of the downstream impinging jets (streamwise nozzles No. 4-6) is larger than that of the upstream impinging jets (streamwise nozzles No. 1-3). When the combined Figure 10(d) and (e), respectively for streamwise nozzles No. 2, 4, 6 and streamwise nozzles No. 1, 3, 5, are compared to Figure 9(d) for streamwise in-line nozzles No. 1-6, deflection of the impinging jets for the staggered jet arrangement in Figure 10 is noticeably larger than the case for the in-line jet arrangement. The most prominent deflection appears for the impinging jets at the last nozzle of the staggered configuration (streamwise nozzle at columns No.6).

The flow characteristics of impinging jets on Z-X plane near the impinged wall (1 mm above the wall) for *Re*=13,400 are shown in Figure 11. The velocity vector and contour in the Y-axis are shown along the location of each orifice. The Y-component velocity represents the velocity in the direction normal to the impingement surface. Its positive direction is towards the downstream of the jet that impinges on the wall. The velocity in the region near each center of impingement is high; impingement regions having velocity higher than 0.5 m/s are clearly seen around the centers of impingement. The impingement surface positioned below the jet having the maximum Y-component velocity in each cell is designated the stagnation point.

The impingement regions in the case of in-line arrangement, shown in Figure 11(a), are clearly shifted towards the downstream direction due to the effect of crossflow. The displacement of each stagnation region (the distance from the centerline of each orifice to the stagnation point of each cell) increases along the downstream direction. These deflections are, however, larger for the case of staggered arrangement as shown in Figure 11(b). Moreover, the stagnation regions of the downstream impinging jets (in column No. 5 and 6) for the staggered arrangement cannot be identified due to strong collision of the crossflow on the jets before impingement.

Flow visualization of jets on the impingement surface using the oil film technique is shown in Figure 12. The black

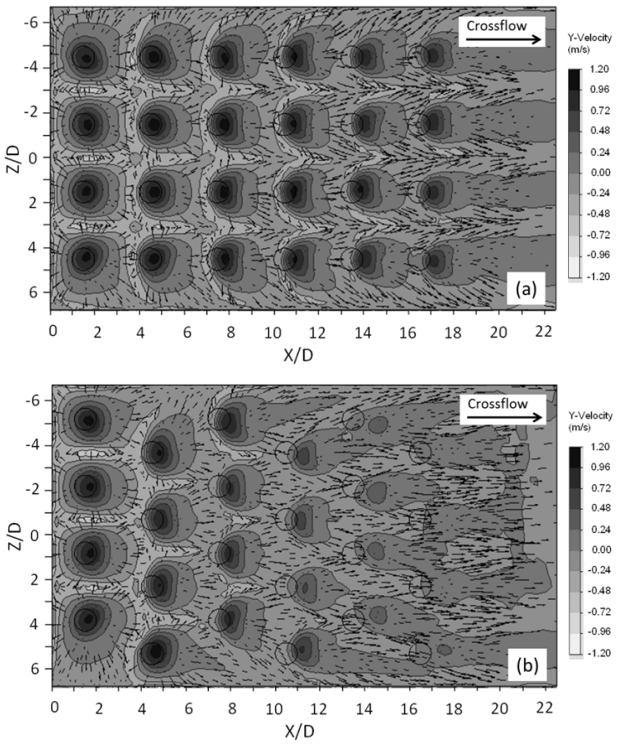

Figure 11. Flow characteristics on Z-X plane near the impinged wall (1 mm above the wall) for Re=13,400: (a) In-line arrangement and (b) staggered arrangement.

and white regions represent the areas where the oil film is completely blown off and the area with original oil film coating, respectively. The cluster of white spots in the middle of the black area in each impinging cell represents the stagnation point of the impinging jet bounded in the jet impingement region. The flow patterns of both the in-line and staggered arrangements agree well with the contours of velocity in the Y-component near the impingement surface shown earlier in Figure 11.

The impingement region of each cell expands in the downstream direction and contracts in the upstream direction for the case of the in-line arrangement, as shown in Figure 12(a). Expansions of impingement regions in the downstream direction are more obvious further downstream to the

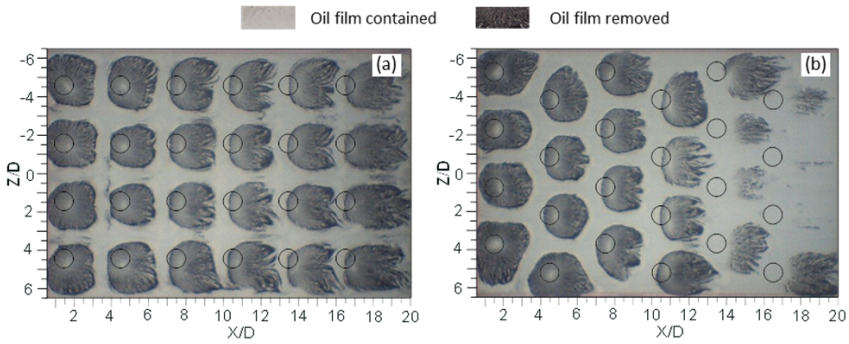

Figure 12. Flow patterns on the impingement surface with oil film technique for Re=13,400: (a) In-line arrangement and (b) staggered arrangement.

channel exit. This characteristic of the flow pattern agrees with the flow visualization study of multiple jets investigated by Brizzi *et al*. (2000).

The impingement regions of the in-line arrangement in Figure 12(a) obviously express themselves throughout all orifice locations while they express indistinctly especially for columns No. 5 and 6 in the case of staggered arrangement as shown in Figure 12(b). This is due to strong deflection of the jets before impingement in the location of jet columns No. 5 and 6 as previously shown in Figure 10(d) and (e).

The effect of crossflow on jet impingements for the staggered arrangement is stronger than the case for the in-line arrangement. Schematic outlines of the flow patterns of crossflow that meander through the jets for the in-line and staggered arrangements are shown in Figure 13. The crossflow passes easily through channels between the rows of jets in the case of in-line arrangement, whereas crossflow from a former column of impinging jets strongly exerts impact on the downstream impinging jets in the case of staggered arrangement.

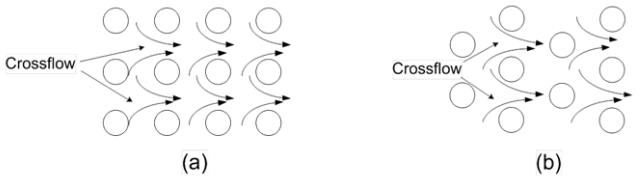

Figure 13. Schematic outlines of crossflow characteristics through difference of jet arrangement: (a) In-line arrangement and (b) staggered arrangement.

3.2 Heat transfer characteristics on impingement surface

The contours of local Nusselt number on the impingement surface for *Re*=13,400 are shown in Figure 14, and the local Nusselt number distributions along X-axis at different Z/D are shown in Figure 15. The contours of Nusselt number in Figure 14 correspond to the flow patterns on the impingement surface in Figure 12, as well as the contours of velocity in Y-component near the impingement surface in Figure 11.

In the case of in-line arrangement shown in Figure 14(a) the Nusselt number is higher at the inner impingement region and becomes lower around the outer region. The area of high Nusselt number in each impingement cell shifts to the downstream direction (X-axis direction) and tends to contract in the spanwise direction (Z-axis direction); the further along downstream to the channel exit, the more. Figure 15 shows the plots of Nusselt number versus X/D for both jet arrangements but at different Z/D indicated dash line in Figure 14. The peak Nusselt number at each impingement region increases continuously from column No. 1 to column No. 4 for the in-line case at Z/D=1.5 (note the black bold solid line peaks in the figure). The highest peak Nusselt number, approx. *Nu*=190, takes place at column No. 4 and the peak decreases again for columns No. 5 and 6. This characteristic of peak Nusselt number at stagnation regions agrees with the result of Katti and Prabhu (2008) in the case of jet-to-plate distance $H \leq 2D$.

This result can be explained by the effect of crossflow velocity on the jet impingement flow. The Nusselt number at the stagnation point in the case of in-line arrangement is increased by the interaction of crossflow with moderate velocity on jet impingement. It can be attributed that turbulent intensity of the jet is increased by the moderate velocity of crossflow. However, in the case of high crossflow velocity, the jet is deflected downstream, so the peak Nusselt number at stagnation region decreases due to low momentum of jet impinging on the surface. This takes place at columns No. 5 and 6.

The Nusselt number distributions in the upstream regions (from columns No. 1 to No. 3) for the staggered arrangement (Figure 14(b)) are not much different when compared to the case of the in-line arrangement (Figure 14 (a)) at same locations. However, the Nusselt number decreases rapidly for the downstream regions (from columns No. 4 to No. 6) of the staggered arrangement because of direct collision of high crossflow velocity with the downstream jets. So, the jets are strongly deflected downstream without impingement as previously mentioned. This results in apparently no stagnation region in the last column of flow visualization in Figure 11(b) and 12(b).

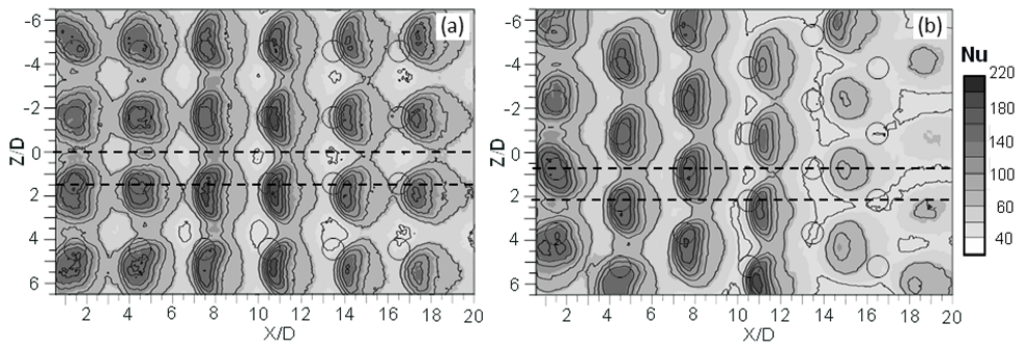

Figure 14. Nusselt number distributions on the impingement surface for Re=13,400 (T_j=27°C): (a) In-line arrangement and (b) staggered arrangement.

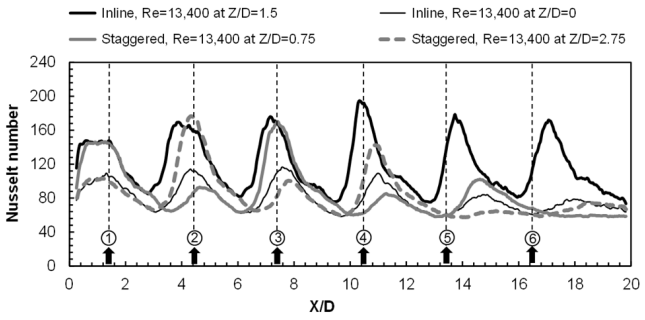

Figure 15. Local Nusselt number distributions along streamwise direction at different Z/D (from dash line in Figure 14 and each arrow indicates the location of orifice).

Figure 16 shows the distributions of spanwise average Nusselt number for the case of *Re*=5,000, 7,500 and 13,400. This average number is calculated by averaging all local wall temperatures in the Z-axis at a particular X/*D*. Results show that the spanwise average Nusselt number of the in-line arrangement is generally larger than that in the case of staggered arrangement for all Reynolds number, and certainly for region X/*D*>7. The peak spanwise average Nussult number for each impingement region decreases monotonically along the downstream direction in the case of staggered arrangement, whereas for the case of in-line arrangement it tends to increase from jet column No. 1 to No. 3 and then decrease monotonically along the downstream direction to the channel exit. This result corresponds to the local heat transfer enhancement in the impingement region for jets at column No. 3 of the in-line arrangement.

3.3 Average Nusselt number

Variations of the average Nusselt number on the impingement surface calculated from the average local wall temperature for the entire surface versus the Reynolds number are shown in Figure 17. The average Nusselt number of both the in-line and staggered arrangements increases as the Reynolds number increases. The average Nusselt number of the in-line arrangement is higher than that of the staggered arrangement throughout all Reynolds numbers. It has been worked out that the average Nusselt number in the case of in-line arrangement is larger than the case of staggered arrangement by approx. 13-20% in the 5,000-13,400 Reynolds number range in this study.

4. Conclusions

In this study, the effects of jet arrangement on the flow and heat transfer characteristics on a surface under two arrays of jet impingement have been experimentally and numerically investigated. The main results for the in-line and staggered arrangements are as follows:

1. The flow characteristics on the impingement surface from the experiment agree well with numerical results: the area of high velocity in the Y-component corresponds to its impingement region, and the area of peak velocity in the Y-component corresponds to the stagnation point of each impinging jet. The impingement region in each cell extends more with further distance towards the downstream direction and contracts more with distance towards the upstream one. This flow pattern of impinging jets coincides with the local Nusselt number distribution on the impingement surface.

2. The effect of crossflow on the jet in the staggered arrangement is stronger than that for the in-line arrangement. Crossflow can easily pass through the gaps between the rows of in-line jets, whereas it appears to be directly blocked by the downstream jet in the case of staggered arrangement. The last column of the staggered jets is most affected by the high crossflow velocity and deflects more to the downstream direction.

3. Moderate crossflow velocity can increase the peak heat transfer of jet impingement. This heat transfer behavior is attributed to the interaction of moderate crossflow velocity that collides with the jet and increases the turbulent intensity of the jet before impingement. However, in the case of high crossflow velocity, the peak heat transfer decreases due to the low momentum of the jet before impingement.

4. The average Nusselt number of the in-line arrangement is approximately 13-20% higher than that of the staggered arrangement in the 5,000-13,400 Reynolds number range.

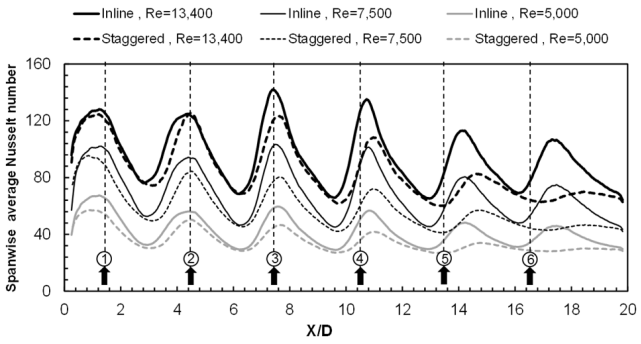

Figure 16. Spanwise average Nusselt number (vertical arrows indicate the locations of column jets).

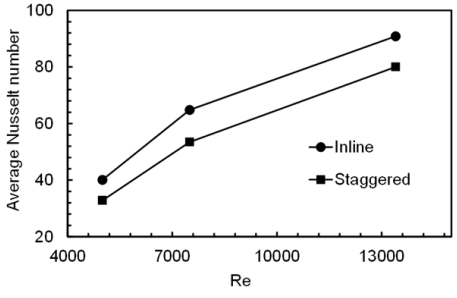

Figure 17. Average Nusselt number for overall impingement surface.

Acknowledgments

This research is co-supported by grants from the Thailand Energy Policy and Planning Office, Ministry of Energy, the Graduate School of the Prince of Songkla University (PSU), and the PSU Faculty of Engineering.

References

Ashforth-Frost, S. and Jambunathan, K. 1996. Effect of nozzle geometry and semi-confinement on the potential core of a turbulent axisymmetric free jet. International Communications in Heat and Mass Transfer. 23(2), 155-162.

Barata, J.M.M. and Durao, D.F.G. 2004. Laser-Doppler measurements of impinging jet flows through a cross-flow. Experiments in Fluids. 36(6), 665-674.

Bouchez, J.-P. and Goldstein, R.J. 1975. Impingement cooling from a circular jet in a cross flow. International Journal of Heat and Mass Transfer. 18(6), 719–730.

Brizzi, L.-E., Bernard, A., Bousgarbies, J.-L., Dorignac, E. and Vullierme, J.-J. 2000. Study of several impinging jets. Journal of Thermal Science. 9(3), 217-223.

Carcasci, C. 1999. An experimental investigation on air impinging jets using visualization methods. International Journal of Thermal Sciences. 38(9), 808-818.

Caliskan, S. and Baskaya, S. 2012. Experimental investigation of impinging jet array heat transfer from a surface with V-shaped and convergent-divergent ribs. International Journal of Thermal Sciences. 59, 234-246.

Colucci, D.W. and Viskanta, R. 1996. Effect of nozzle geometry on local convective heat transfer to a confined impinging air jet. Experimental Thermal and Fluid Science. 13(1), 71-80.

Florschuetz, L.W., Truman, C.R. and Metzger, D.E. 1981. Streamwise flow and heat transfer distributions for jet array impingement with crossflow. ASME Journal of Heat Transfer. 103, 337-342.

Geers, L.F.G., Tummers, M.J., Bueninck, T.J. and Hanjalic, K. 2008. Heat transfer correlation for hexagonal and in-line arrays of impinging jets. International Journal of Heat and Mass Transfer. 51, 5389-5399.

Goldstein, R.J. and Behbahani, A.I. 1982. Impingement of a circular jet with and without crossflow. International Journal of Heat and Mass Transfer. 25(9), 1377-1382.

Hoberg, T.B., Onstad, A.J. and Eaton, J.K. 2010. Heat transfer measurements for jet impingement arrays with local extraction. International Journal of Heat and Fluid Flow. 31, 406-467.

Katti, V. and Prabhu, S.V. 2008. Influence of spanwise pitch on local heat transfer distribution for in-line arrays of circular jets with spent air flow in two opposite directions. Experimental Thermal and Fluid Science. 33(1), 84-95.

Nakabe, K., Suzuki, K., Inaoka, K., Higashio, A., Acton, J.S. and Chen, W. 1998. Generation of longitudinal vortices in internal flows with an inclined impinging jet and enhancement of target plate heat transfer. International Journal of Heat and Fluid Flow. 19(5), 573-581.

Nuntadusit, C., Wae-hayee, M., Bunyajitradulya, A. and Eiamsa-ard, S. 2012a. Heat transfer enhancement by multiple swirling impinging jets with twisted-tape swirl generators. International Communications in Heat and Mass Transfer. 39(1), 102-107.

Nuntadusit, C., Wae-hayee, M., Tekasakul, P. and Eiamsa-ard, S. 2012b. Local heat transfer characteristics of array impinging jets from elongated orifices. International Communications in Heat and Mass Transfer. 39(8), 1154-1164.

Rallabandi, A.P., Rhee, D.-H., Gao, Z. and Han, J.-C. 2010. Heat transfer enhancement in rectangular channels with axial ribs or porous foam under through flow and impinging jet conditions. International Journal of Heat and Mass Transfer. 53(9), 4663-4671.

Shi, Y., Ray, M.B. and Mujumdar, A.S. 2003. Numerical study on the effect of crossflow on turbulent flow and heat transfer characteristics under normal and oblique semi-confined impinging slot jets. Drying Technology. 21(10), 1923-1939.

Versteeg, H.K. and Malalasekera, W. 1995. An introduction to computational fluid dynamics: The finite volume method. Longman Scientific & Technical, England. 133-155.

Viskanta, R. 1993. Heat transfer to impinging isothermal gas and flame jets. Experimental Thermal and Fluid Science. 6(2), 111-134.

Xing, Y., Spring, S. and Weigand, B. 2011. Experimental and numerical investigation of impingement heat transfer on a flat and micro-rib roughened plate with different crossflow schemes. International Journal of Thermal Sciences. 50(7), 1293-1307.

Yang, Y.-T. and Wang, Y.-X. 2005. Three-dimensional numerical simulation of an inclined jet with cross-flow. International Journal of Heat and Mass Transfer. 48, 4019-4027.